

Cortical plasticity induced by transplantation of embryonic somatostatin or parvalbumin interneurons

Yunshuo Tang^{a,b,c,d,1}, Michael P. Stryker^{e,f,g,2}, Arturo Alvarez-Buylla^{c,d,2}, and Juan Sebastian Espinosa^{e,f,g,1,2}

^aMedical Scientist Training Program and ^bBiomedical Sciences Graduate Program, ^dThe Eli and Edythe Broad Center of Regeneration Medicine and Stem Cell Research, ^cCenter for Integrative Neuroscience, and Departments of ^eNeurological Surgery, ^fPhysiology, and ^gBioengineering and Therapeutic Sciences, University of California, San Francisco, CA 94143

Contributed by Michael P. Stryker, November 14, 2014 (sent for review September 13, 2014; reviewed by Oscar Marin and Joshua T. Trachtenberg)

GABAergic inhibition has been shown to play an important role in the opening of critical periods of brain plasticity. We recently have shown that transplantation of GABAergic precursors from the embryonic medial ganglionic eminence (MGE), the source of neocortical parvalbumin- (PV⁺) and somatostatin-expressing (SST⁺) interneurons, can induce a new period of ocular dominance plasticity (ODP) after the endogenous period has closed. Among the diverse subtypes of GABAergic interneurons PV⁺ cells have been thought to play the crucial role in ODP. Here we have used MGE transplantation carrying a conditional allele of diphtheria toxin alpha subunit and cell-specific expression of Cre recombinase to deplete PV⁺ or SST⁺ interneurons selectively and to investigate the contributions of each of these types of interneurons to ODP. As expected, robust plasticity was observed in transplants containing PV⁺ cells but in which the majority of SST⁺ interneurons were depleted. Surprisingly, transplants in which the majority of PV⁺ cells were depleted induced plasticity as effectively as those containing PV⁺ cells. In contrast, depleting both cell types blocked induction of plasticity. These findings reveal that PV⁺ cells do not play an exclusive role in ODP; SST⁺ interneurons also can drive cortical plasticity and contribute to the reshaping of neural networks. The ability of both PV⁺ and SST⁺ interneurons to induce de novo cortical plasticity could help develop new therapeutic approaches for brain repair.

medial ganglionic eminence | parvalbumin interneuron | somatostatin interneuron | critical period | ocular dominance plasticity

Critical periods of activity-dependent plasticity shape the early development of many cortical areas. GABAergic inhibition has been shown to play an important role in the opening of a critical period in the developing visual cortex during which monocular visual deprivation (MD) rapidly alters the balance of responses to the two eyes (1–3). This ocular dominance plasticity (ODP) takes place with a well-defined beginning and end. The majority of GABAergic interneurons in the neocortex are derived from the medial ganglionic eminence (MGE) (4–8). Transplantation of embryonic inhibitory neuronal precursors from the MGE into the visual cortex of postnatal animals can induce a second window of plasticity (9). The transplanted interneurons, consisting primarily of parvalbumin-expressing (PV⁺) and somatostatin-expressing (SST⁺) cells, disperse, mature, and integrate into local visual cortical circuit (10–12). Evidence to date links only the PV⁺ interneurons to ODP (13–15). SST⁺ interneurons have scarcely been studied in the context of ODP despite their abundance in the visual cortex and their powerful influence on the apical dendrites of pyramidal cells (16, 17). Here we take advantage of MGE transplantation to dissect the contributions of different types of cortical interneuron cells to plasticity. We genetically ablated PV⁺ or SST⁺ cells in the transplants and tested whether the transplanted cells induced a second critical period in the recipients. Removing either PV⁺ or SST⁺ cells did not hinder the ability of MGE transplants to induce ODP, but removing both eliminated the plasticity. These results demonstrate that PV⁺ cells do not play an exclusive role

in ODP; SST⁺ cells also can drive plasticity and reshape neural circuits when the majority of PV⁺ cells are eliminated. Furthermore, the ODP induced by MGE transplants resembled the plasticity in the normal critical period and differed from the plasticity observed in older animals in its magnitude, its sensitivity to brief MD, and in the weakening of response to the deprived eye. These findings reveal specific cortical GABAergic-inhibitory cell types that mediate plasticity.

Results

We devised a genetic strategy to deplete PV⁺ or SST⁺ interneurons selectively in MGE transplants through the use of mice expressing Cre recombinase under the control of the endogenous PV and SST promoters (*PV-cre* and *SST-cre*, respectively) (18, 19). When we examined the MGE at embryonic day (E) 14, no expression of a fluorescent reporter was detected in *PV-cre* or *SST-cre* mice, precluding the use of fluorescence cell sorting to transplant pure populations of PV⁺ or SST⁺ cells. Therefore, we elected to eliminate PV⁺ populations, SST⁺ populations, or both after transplantation and then study the effects of their absence on transplant-induced plasticity. Diphtheria toxin alpha subunit (DTA) is a potent intracellular toxin that induces programmed cell death within 48 h of expression by blocking protein synthesis (20). We crossed *PV-cre* and *SST-cre* mice to transgenic mice harboring a Cre-inducible DTA allele (*R26-DTA*) to achieve targeted depletion of PV⁺ and SST⁺ cells, respectively. The *R26-DTA* mice also express GFP ubiquitously, permitting the visualization of transplanted cells (21). We found *PV-cre;R26-DTA* (PV-depleted) and *SST-cre;R26-DTA* (SST-depleted) mice to be largely perinatal lethal, but E13.5 embryos from both crosses were of normal size and gross appearance. We next transplanted MGE cells from PV-depleted, SST-depleted, and *PV-cre;SST-cre;R26-DTA*

Significance

The cerebral cortex contains two major types of interneurons that are implicated in epilepsy and neurodegenerative diseases. Here we determined their role in the induction of critical period plasticity, a form of circuit modification essential for brain maturation and repair. Surprisingly, transplantation of either cell type was sufficient to induce critical period plasticity. The work provides insight into the cellular mechanisms that shape brain circuits during key periods of development and defines populations of inhibitory nerve cells sufficient to induce plastic changes that could help in the treatment of brain diseases.

Author contributions: Y.T., M.P.S., A.A.-B., and J.S.E. designed research; Y.T. and J.S.E. performed research; Y.T., M.P.S., A.A.-B., and J.S.E. analyzed data; and Y.T., M.P.S., A.A.-B., and J.S.E. wrote the paper.

Reviewers: O.M., King's College, London; and J.T.T., University of California, Los Angeles. The authors declare no conflict of interest.

¹Y.T. and J.S.E. contributed equally to this work.

²To whom correspondence may be addressed. Email: stryker@phy.ucsf.edu, abuylla@stemcell.ucsf.edu, or sebastian@phy.ucsf.edu.

This article contains supporting information online at www.pnas.org/lookup/suppl/doi:10.1073/pnas.1421844112/-DCSupplemental.

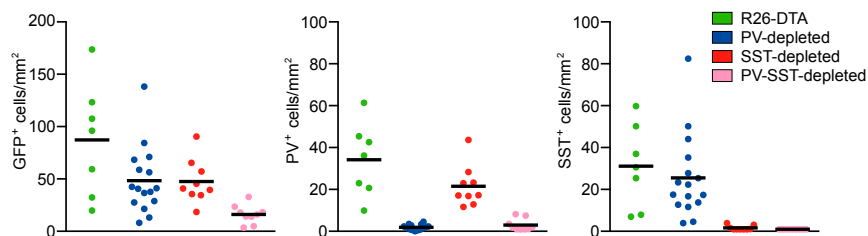


Fig. 2. Depletions of PV⁺ and SST⁺ cells cause reciprocal enrichment but do not affect the absolute population size of each other in the transplant. Density (cells per square millimeter) of total GFP⁺ cells (Left), PV⁺ cells (Center), and SST⁺ cells (Right) in R26-DTA ($n = 7$), PV-depleted ($n = 16$), SST-depleted ($n = 9$), and PV-SST-depleted ($n = 9$) transplants. Horizontal bars indicate mean.

despite the death of the majority of transplanted cells (Fig. S3). These findings show that selectively ablating PV⁺ or SST⁺ cells by DTA efficiently eliminated the target population without affecting the survival or migration of the remaining cells.

After characterizing the PV- and SST-depleted MGE transplants, we examined whether these transplants could induce a second critical period of plasticity. Using intrinsic signal optical imaging, we tested recipients of PV-depleted, SST-depleted, PV-SST-depleted, control R26-DTA, or freeze-thaw-killed MGE cells for plasticity at 33–35 DAT, when the transplanted cells were at an equivalent age of P26–P28 and displayed the greatest ability to induce plasticity (9). As expected, R26-DTA MGE transplants induced robust plasticity, whereas dead MGE transplants did not. Surprisingly, PV-depleted and SST-depleted transplants each induced rapid and robust plasticity. On the other hand, recipients of PV-SST-depleted transplants, in which

both PV⁺ and SST⁺ cells had been killed, did not show plasticity (Fig. 3A and Table S1). Comparing the plasticity induced by PV-depleted, SST-depleted, and control R26-DTA transplants, we found that all three types of transplants induced plasticity of similar magnitude (Fig. 3B). Because the efficiency of combined Cre and DTA expression is not 100%, a few PV⁺ or SST⁺ cells were present in the selectively depleted transplants. PV⁺ cells, especially, are known to develop extensive axonal arbors with hundreds of postsynaptic targets, suggesting that a small population of PV⁺ cells might be sufficient to induce changes in circuitry. If plasticity depended on PV⁺ cells alone, the required density would have to be greater than approximately eight cells/mm² (Fig. 3C, Center), the maximum density of PV⁺ cells in transplants that did not induce plasticity. The PV⁺ cell density in PV-depleted transplants was always less. That is, the density of surviving PV⁺ cells in the PV-SST-depleted transplants that did

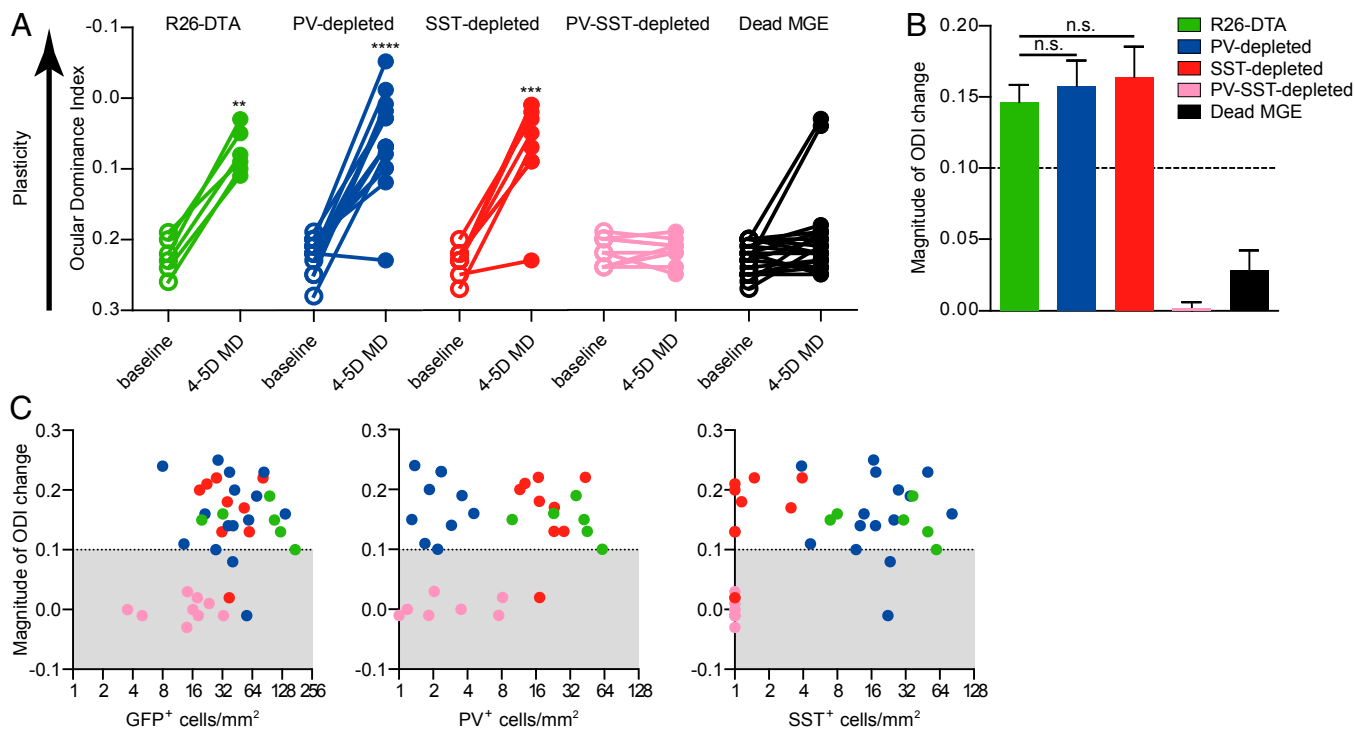


Fig. 3. MGE transplants depleted of PV⁺ or SST⁺ cells, but not of both cell types, are capable of inducing plasticity. (A) ODI before and after MD of the contralateral eye in recipients of PV-depleted ($n = 16$), SST-depleted ($n = 9$), PV-SST-depleted ($n = 9$), or dead cells ($n = 20$) transplants. Lower values of ODI after deprivation indicate greater plasticity. $**P < 0.01$, $***P < 0.001$, $****P < 0.0001$ (Mann–Whitney–Wilcoxon rank-sum test). (B) Change in ODI is similar among R26-DTA ($n = 7$), PV-depleted ($n = 16$), and SST-depleted ($n = 9$) transplants. Error bars represent SEM. The line at 0.1 indicates the threshold for plasticity. n.s., not significant (one-way ANOVA and Bonferroni post hoc test). (C) Linear regression analysis shows that the magnitude of ODI change is not related to the density of total GFP⁺ cells ($n = 39$, slope = 0.0006, $r^2 = 0.07$, n.s.) (Left), of PV⁺ cells ($n = 39$, slope = 0.0012, $r^2 = 0.05$, n.s.) (Center), or of SST⁺ cells ($n = 39$, slope = 0.0013, $r^2 = 0.08$, n.s.) (Right). Shaded region indicates little or no plasticity.

not induce plasticity was similar to or greater than that in PV-depleted transplants that did induce plasticity. This finding makes it implausible that the surviving PV⁺ cells were responsible for the plasticity (Fig. 2, *Center*), although they may have participated in the plasticity induced in the presence of normal numbers of transplant-derived SST⁺ cells. Furthermore, pooling cell density from all transplant types revealed no correlation between the magnitude of plasticity induced by MGE transplantation and the average densities or rostral–caudal distribution of total surviving transplanted cells, of transplanted PV⁺ cells, or of transplanted SST⁺ cells (Fig. 3C, *x* axis expanded logarithmically to display low cell densities, and Fig. S4). These results show that MGE transplants with normal numbers of transplanted SST⁺ cells are sufficient to induce plasticity when more than 95% of the PV⁺ cells are depleted.

The maturation of GABAergic interneurons, specifically of the PV⁺ subtype that derives predominantly from the MGE, has been strongly implicated in critical period plasticity. Therefore it was surprising that transplanted MGE interneuron precursors depleted of PV⁺ cells were still competent for plasticity. One possible explanation would be that the plasticity induced by MGE transplants is not critical period plasticity but merely is an enhancement of adult ODP. To test this hypothesis, we examined several features of plasticity that differentiate critical period plasticity from adult plasticity (22). First, the onset of plasticity after only 4–5 d of deprivation is consistent with critical period plasticity, in contrast to adult plasticity, which takes 7–8 d of deprivation to produce significant shifts in the ocular dominance index (ODI). Second, transplant-induced plasticity was driven primarily by the loss of contralateral responsiveness, which is a key feature of critical period plasticity that is not observed in the adult form of ODP (Fig. 4A). Finally, the degree of loss of contralateral response was similar following PV-depleted, SST-depleted, and control *R26-DTA* transplants; it also was not influenced by the number of PV⁺ or SST⁺ cells in the transplant (Fig. 4B, *x* axis expanded logarithmically). The plasticity induced by MGE transplants shares the rapid depression of contralateral response characteristic of critical period plasticity, and normal numbers of PV⁺ interneurons are not required for this phenomenon.

Discussion

In this study we used Cre-DTA to deplete PV⁺ or SST⁺ interneurons from MGE transplants. When MGE-derived interneuron precursors were genetically programmed to undergo apoptosis upon expression of Cre recombinase from the PV or SST locus, almost all the corresponding Cre-expressing interneurons

were eliminated from the transplant before the window of induction for plasticity opened (Figs. 1 and 2). Despite the depletion of PV⁺ or SST⁺ cells, these transplants retained their ability to induce ODP, which was indistinguishable from control transplants. However, when both PV⁺ and SST⁺ populations were eliminated simultaneously, the remaining cells failed to induce plasticity (Fig. 3), suggesting that either PV⁺ or SST⁺ cells need to be present in normal numbers in the transplant for plasticity to occur. However, although both PV⁺ and SST⁺ cells are competent to induce critical period-like ODP, other interneurons derived from the MGE appear not to be.

Studies over the last decade have suggested that PV⁺ cells play an exclusive role in initiating critical period ODP. GABA_A receptors containing the $\alpha 1$ subunit, which is enriched at PV⁺ synapses, have been shown to play a particularly potent role in the opening of the critical period of ODP (2). In other studies, manipulating factors that affect the maturation of PV⁺ cells also affected the opening of the critical period of ODP, including polysialylated neural cell adhesion molecule (PSA-NCAM), the homeoprotein transcription factor orthodenticle homolog 2 (*Otx2*), and insulin-like growth factor 1 (*IGF1*) (13, 23, 24). PV⁺ cells' electrophysiological activity also has been implicated in plasticity; depressing the activity of PV⁺ cells a few days after the critical period increased plasticity in primary visual cortex (14). Consistent with these findings, our data support the capacity of PV⁺ cells to drive plasticity. However, our results are inconsistent with an exclusive role for PV⁺ cells in this process.

Our finding that transplants depleted of PV⁺ cells also could induce robust plasticity but those depleted of both PV⁺ and SST⁺ cells could not suggests that SST⁺ cells also can drive plasticity, a possibility that largely has been ignored. Although our findings concern plasticity after the critical period, they raise the possibility that SST⁺ cells also may be important during the critical period. Indeed, it is unknown whether in previous studies in which PV⁺ cells were manipulated to modify ODP, SST⁺ cells also were affected.

Signals that are part of the immune response can affect plasticity in the visual pathway (25, 26), including ODP (27, 28). Although cell death in our depletion experiments might stimulate an immune response, our PV-SST-depleted transplants, which presumably had an immune response similar to or greater than that of PV-depleted or SST-depleted transplants, did not induce plasticity. Thus, the plasticity induced by PV-depleted and SST-depleted transplants was unlikely to result from the killing of transplanted cells or from a nonspecific immune response from the host. Instead, plasticity appears to be a direct

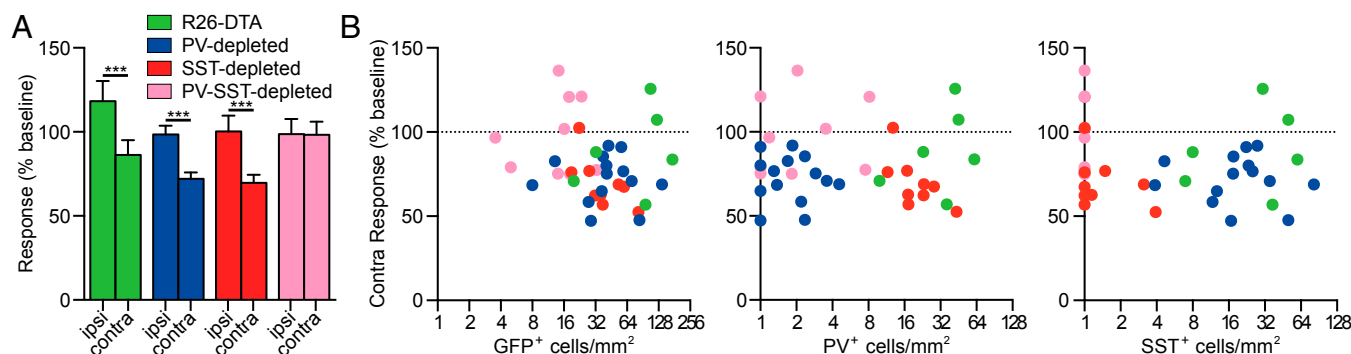


Fig. 4. Critical period-like characteristics of transplant-induced plasticity. (A) Changes in magnitude of ipsilateral and contralateral responses after deprivation, expressed as percentage of pre-MD baseline values, in *R26-DTA* ($n = 7$), PV-depleted ($n = 14$), SST-depleted ($n = 9$), and PV-SST-depleted ($n = 9$) transplants. Error bars represent SEM. *** $P < 0.001$ (Mann–Whitney–Wilcoxon rank-sum test). (B) Linear regression analysis shows that the change in the magnitude of the contralateral response is unrelated to the density of total GFP⁺ cells ($n = 39$, slope = -0.045 , $r^2 = 0.0066$, n.s.) (Left), of PV⁺ cells ($n = 39$, slope = 0.011 , $r^2 = 0.00006$, n.s.) (Center), or of SST⁺ cells ($n = 39$, slope = -0.1085 , $r^2 = 0.01$, n.s.) (Right). The dotted line indicates 100% of baseline.

result of neural circuit modification induced by the transplanted PV⁺ and SST⁺ cells that integrate into primary visual cortex.

What mechanism of plasticity might be shared between PV⁺ and SST⁺ cells? Studies of connectivity show that transplanted MGE cells make and receive profuse connections, about three times as many as host inhibitory neurons at the peak of the transplant-induced critical period (9). The intercalation of such new connections into a cortical circuit that otherwise would be stable to perturbations of visual input may be sufficient to push it out of its zone of stability. Any inhibitory neurons that made sufficiently profuse connections then might suffice to induce plasticity. Alternatively, PV⁺ and SST⁺ cells, but not the other cells of the MGE transplants, might contain factors that alter the extracellular matrix or influence perineuronal nets. Our delineation of the responsible cells is an important step toward understanding the mechanism of transplant-induced plasticity, even though the actual mechanism still is not clear.

Generation of PV⁺ and SST⁺ cells is not always synchronized spatially or temporally during development (8, 29). For instance, in addition to the MGE, the preoptic area also generates PV⁺ cells that reach the visual cortex (30). Indeed, although the mouse primary visual cortex contains more PV⁺ interneurons than SST⁺ interneurons (16), MGE transplantation yields approximately equal numbers of PV⁺ and SST⁺ cells (9).

Cortical plasticity plays important roles in normal development and has significant implications in disease (e.g., in amblyopia) and in injury repair (e.g., in stroke and trauma rehabilitation) (31–33). MGE transplantation is being developed as a promising therapeutic modification of neural circuits in several diseases (34). Identifying and understanding the roles that different interneuron subtypes play in plasticity will yield insight into the mechanisms responsible for plasticity and will guide the therapeutic application of interneuron transplantation.

Methods

Transgenic Animals. The Institutional Animal Care and Use Program at the University of California, San Francisco approved all protocols and procedures. All mice were housed in standard conditions on a 12-h dark/light cycle in the Laboratory Animal Resource Center at the University of California, San Francisco. *PV-cre*, *SST-cre*, *R26-DTA*, *Ai14*, and wild-type C57BL/6J breeders were purchased from The Jackson Laboratory. Donor MGE cells were produced by crossing *PV-cre/Ai14* double-homozygous, *SST-cre/Ai14* double-homozygous, or *PV-cre/SST-cre/Ai14* triple-homozygous mice to *R26-DTA* homozygous mice and harvesting the embryos at E13.5. Recipient animals were obtained from breeding wild-type C57BL/6J animals together.

Cell Dissection and Transplantation. The ventricular and subventricular zones of the MGE were dissected from E13.5 donor embryos and dissociated into single cells via repeated pipetting in Leibovitz's L-15 medium containing 100 IU/mL DNase I (Roche). Cells then were concentrated by centrifugation at 600 × *g* for 3 min. P7 C57BL/6J recipients were anesthetized using hypothermia until pedal reflex disappeared and then were placed on a stereotaxic injection platform. The concentrated cells (~100,000 cells/μL) were loaded into a beveled Drummond glass micropipette (Drummond Scientific) that was positioned at 30° from vertical. Two injections were placed into the caudal left cortex with the coordinates anterior–posterior (A–P) 7 mm, medial–lateral (M–L) 3.5 mm and A–P 6.5 mm, M–L 3.2 mm, respectively. Zero was defined as the inner corner of the eye for A–P and as the midpoint between two eyes M–L. The depth of both injections was 1.3 mm from the surface of the skin. After injections, recipients were placed on a heating pad until they became warm and active. Mice subsequently were returned to their mothers until weaning age (P21).

Immunostaining. Animals were perfused with 4% formaldehyde in PBS. The brains were removed, postfixed for 2 h in 4% formaldehyde, and cryoprotected in 30% sucrose. Coronal sections (30 μm) were cut using a sliding microtome (Leica & Physitemp Instruments). Free-floating sections were blocked for 1 h at room temperature in blocking solution [Tris-buffered saline (TBS), 10% normal donkey serum, and 1% Tween-100] and were incubated at 4 °C overnight using the following primary antibodies: chicken

anti-GFP, 1:1,000 (Aves); mouse anti-PV, 1:1,000 (Sigma); rabbit anti-SST, 1:300 (Swant); goat anti-SST, 1:200 (Santa Cruz); rabbit anti-calbindin, 1:1,000 (Millipore); rabbit anti-calretinin, 1:1,000 (Millipore); rabbit anti-neuropeptide Y (NPY), 1:1,000 (Abcam); and rabbit anti-Reelin, 1:1,000 (Abcam). After washing in TBS and 1% Tween-100 three times for 15 min each, sections were incubated in blocking solution with the following secondary antibodies at 1:1,000 each: Alexa Fluor 488 donkey anti-chicken (Jackson ImmunoResearch), Alexa Fluor 568 donkey anti-mouse, Alexa Fluor 568 donkey anti-rabbit, Alexa Fluor 647 donkey anti-rabbit, and Alexa Fluor 647 donkey anti-goat (Life Technologies). After 1 h of incubation with secondary antibodies at room temperature, sections were washed three times in PBS for 10 min each, mounted on glass slides, and coverslipped.

Cell Quantification. Images of the binocular visual cortex, demarcated by the Dil (1,1'-Diiodo-3,3',3'-Tetramethylindocarbocyanine perchlorate) injections, were captured using the Zeiss Axiovert-200 microscope (Zeiss), a AxioCam MRm camera (Zeiss), and Neurolucida (MBF Bioscience). GFP⁺ cells were counted in every sixth section (180 μm apart). To determine cell densities, all GFP⁺ cells within the binocular visual cortex were counted, and these numbers were divided by the area of binocular visual cortex delineated by the Dil injections (see below).

Optical Imaging of Intrinsic Signals. Surgical preparation, optical imaging, and analysis of intrinsic signals were performed as previously described (35, 36). Briefly, 2–3 d before imaging, mice were anesthetized using 2.5% isoflurane in oxygen, and the skull over the left visual cortex was exposed and protected with a layer of nitrocellulose (New-Skin; MedTech Products). A custom stainless steel head plate was attached to the skull with dental acrylic. Mice then were given 5 mg/kg of carprofen s.c. for postoperative analgesia. On the day of baseline imaging, mice were anesthetized with 0.7% isoflurane in oxygen, supplemented with a single i.p. injection of 2–5 mg/kg chlorprothixene, and placed on a heating pad that maintained the body temperature at 37.5 °C through a rectal thermo probe feedback. The head plate was secured in a stereotaxic frame, and the imaging window directly above the binocular visual cortex was covered with agarose and topped with a coverslip to provide a flat imaging surface. The eyes were protected with a thin coat of silicone oil. A black-and-white contrast-modulated stochastic noise movie was presented to the binocular visual field (–5° to +15° azimuth) at 25 cm in front of the mice. The movie was presented, four or five times to each eye alternatively for 5 min per session for a total presentation of 20–30 min to each eye. During the imaging sessions, 610-nm light reflected by the visual cortex was gathered using a Dalsa 1M30 CCD camera (Dalsa) focused at 550 μm beneath the surface of the brain. At the end of the last imaging session, the boundaries of the binocular cortex were determined by overlapping the response maps of optical imaging with images of surface blood vessels and were marked with thin tungsten wire coated with Dil (Invitrogen).

Analysis of Optical Imaging Data. A map of visual response data was extracted from the raw optical imaging data using a custom Fourier analysis program (37). The average amplitude of signal within the region corresponding to the binocular visual cortex was taken to represent the strength of visual response. ODI was computed as the average of $(C - I)/(C + I)$ at each pixel within the binocular response region, where *C* is the response to contralateral visual stimulation and *I* is the response to ipsilateral stimulation.

Statistical Analysis of Histological and Optical Imaging Data. A Mann–Whitney–Wilcoxon rank-sum test was performed to determine the significance of differences in ODI at baseline and after 4–5 d MD, the rostral–caudal distribution of transplanted cells, and the degree of plasticity and the amplitude of ocular response for each experimental group. One-way ANOVA and Bonferroni post hoc test was performed to determine the significance of differences in ocular dominance shift (defined as baseline ODI – post MD ODI) among experimental groups. Linear regression was performed to determine the dependency of magnitude of plasticity or amplitude of visual response on the density of total transplanted cells, transplanted PV⁺ cells, or transplanted SST⁺ cells. All statistical analyses were performed using Prism 5 (GraphPad).

ACKNOWLEDGMENTS. We thank J. R. Rodriguez and C. Guinto for technical contributions. This work was supported by the California Institute for Regenerative Medicine Grant TG2-01153 (to A.A.-B.); National Institutes of Health Grants R01EY02874 (to M.P.S.), T32GM007618 (to Y.T.), and K22NS089799 (to J.S.E.); and a University of California President's Postdoctoral Fellowship Program Grant (to J.S.E.).

1. Hensch TK, et al. (1998) Local GABA circuit control of experience-dependent plasticity in developing visual cortex. *Science* 282(5393):1504–1508.
2. Fagioliini M, et al. (2004) Specific GABA circuits for visual cortical plasticity. *Science* 303(5664):1681–1683.
3. Fagioliini M, Hensch TK (2000) Inhibitory threshold for critical-period activation in primary visual cortex. *Nature* 404(6774):183–186.
4. Anderson SA, Eisenstat DD, Shi L, Rubenstein JL (1997) Interneuron migration from basal forebrain to neocortex: Dependence on Dlx genes. *Science* 278(5337):474–476.
5. Wichterle H, Turnbull DH, Nery S, Fishell G, Alvarez-Buylla A (2001) In utero fate mapping reveals distinct migratory pathways and fates of neurons born in the mammalian basal forebrain. *Development* 128(19):3759–3771.
6. Pleasure SJ, et al. (2000) Cell migration from the ganglionic eminences is required for the development of hippocampal GABAergic interneurons. *Neuron* 28(3):727–740.
7. Nery S, Fishell G, Corbin JG (2002) The caudal ganglionic eminence is a source of distinct cortical and subcortical cell populations. *Nat Neurosci* 5(12):1279–1287.
8. Wonders CP, Anderson SA (2006) The origin and specification of cortical interneurons. *Nat Rev Neurosci* 7(9):687–696.
9. Southwell DG, Froemke RC, Alvarez-Buylla A, Stryker MP, Gandhi SP (2010) Cortical plasticity induced by inhibitory neuron transplantation. *Science* 327(5969):1145–1148.
10. Wichterle H, Garcia-Verdugo JM, Herrera DG, Alvarez-Buylla A (1999) Young neurons from medial ganglionic eminence disperse in adult and embryonic brain. *Nat Neurosci* 2(5):461–466.
11. Alvarez-Dolado M, et al. (2006) Cortical inhibition modified by embryonic neural precursors grafted into the postnatal brain. *J Neurosci* 26(28):7380–7389.
12. Hunt RF, Girsakis KM, Rubenstein JL, Alvarez-Buylla A, Baraban SC (2013) GABA progenitors grafted into the adult epileptic brain control seizures and abnormal behavior. *Nat Neurosci* 16(6):692–697.
13. Sugiyama S, et al. (2008) Experience-dependent transfer of Otx2 homeoprotein into the visual cortex activates postnatal plasticity. *Cell* 134(3):508–520.
14. Kuhlman SJ, et al. (2013) A disinhibitory microcircuit initiates critical-period plasticity in the visual cortex. *Nature* 501(7468):543–546.
15. Miyata S, Komatsu Y, Yoshimura Y, Taya C, Kitagawa H (2012) Persistent cortical plasticity by upregulation of chondroitin 6-sulfation. *Nat Neurosci* 15(3):414–422, S411–412.
16. Gonchar Y, Wang Q, Burkhalter A (2008) Multiple distinct subtypes of GABAergic neurons in mouse visual cortex identified by triple immunostaining. *Front Neuroanatomy* 1:3.
17. Spratling MW, Johnson MH (2003) Exploring the functional significance of dendritic inhibition in cortical pyramidal cells. *Neurocomputing* 52–54:389–395.
18. Hippenmeyer S, et al. (2005) A developmental switch in the response of DRG neurons to ETS transcription factor signaling. *PLoS Biol* 3(5):e159.
19. Taniguchi H, et al. (2011) A resource of Cre driver lines for genetic targeting of GABAergic neurons in cerebral cortex. *Neuron* 71(6):995–1013.
20. Choe S, et al. (1992) The crystal structure of diphtheria toxin. *Nature* 357(6375):216–222.
21. Ivanova A, et al. (2005) In vivo genetic ablation by Cre-mediated expression of diphtheria toxin fragment A. *Genesis* 43(3):129–135.
22. Sato M, Stryker MP (2008) Distinctive features of adult ocular dominance plasticity. *J Neurosci* 28(41):10278–10286.
23. Ciucci F, et al. (2007) Insulin-like growth factor 1 (IGF-1) mediates the effects of enriched environment (EE) on visual cortical development. *PLoS ONE* 2(5):e475.
24. Di Cristo G, et al. (2007) Activity-dependent PSA expression regulates inhibitory maturation and onset of critical period plasticity. *Nat Neurosci* 10(12):1569–1577.
25. Schafer DP, et al. (2012) Microglia sculpt postnatal neural circuits in an activity and complement-dependent manner. *Neuron* 74(4):691–705.
26. Stephan AH, et al. (2013) A dramatic increase of C1q protein in the CNS during normal aging. *J Neurosci* 33(33):13460–13474.
27. Syken J, Grandpre T, Kanold PO, Shatz CJ (2006) PirB restricts ocular-dominance plasticity in visual cortex. *Science* 313(5794):1795–1800.
28. Datwani A, et al. (2009) Classical MHC I molecules regulate retinogeniculate refinement and limit ocular dominance plasticity. *Neuron* 64(4):463–470.
29. Inan M, Welagen J, Anderson SA (2012) Spatial and temporal bias in the mitotic origins of somatostatin- and parvalbumin-expressing interneuron subgroups and the chandelier subtype in the medial ganglionic eminence. *Cereb Cortex* 22(4):820–827.
30. Gelman DM, et al. (2009) The embryonic preoptic area is a novel source of cortical GABAergic interneurons. *J Neurosci* 29(29):9380–9389.
31. Sharma N, Classen J, Cohen LG (2013) Neural plasticity and its contribution to functional recovery. *Handb Clin Neurol* 110:3–12.
32. Hosp JA, Luft AR (2011) Cortical plasticity during motor learning and recovery after ischemic stroke. *Neural Plast* 2011:871296.
33. Awaya S, Watanabe Y (1995) Amblyopia. *Curr Opin Ophthalmol* 6(5):9–14.
34. Southwell DG, et al. (2014) Interneurons from embryonic development to cell-based therapy. *Science* 344(6180):1240622.
35. Gandhi SP, Yanagawa Y, Stryker MP (2008) Delayed plasticity of inhibitory neurons in developing visual cortex. *Proc Natl Acad Sci USA* 105(43):16797–16802.
36. Kaneko M, Stryker MP (2014) Sensory experience during locomotion promotes recovery of function in adult visual cortex. *eLife* 3:e02798.
37. Kalatsky VA, Stryker MP (2003) New paradigm for optical imaging: Temporally encoded maps of intrinsic signal. *Neuron* 38(4):529–545.
38. Madisen L, et al. (2010) A robust and high-throughput Cre reporting and characterization system for the whole mouse brain. *Nat Neurosci* 13(1):133–140.